DOI: 10.6977/IJoSI.202312_7(8).0004
V. Shulunov./Int. J. Systematic Innovation, 7(8),37-47(2023)

# Enhanced Roll Porous Scaffold 3D bioprinting technology

Vyacheslav Shulunov

Institute of Physical Materials Science
of the Siberian Branch of the Russian Academy of Science, Ulan-Ude, Russia
Corresponding author E-mail: acoswt@yandex.ru

(Received 2 August 2023; Final version received 21 September 2023; Accepted 12 October 2023)

## Abstract

The upgrade of the Roll Porous Scaffold (RPS) 3D bioproduction technique provides significant advantages over today's dominant analogues. The density 10–15 *μm* cells in the formed object increased up to ~$1.26\times10^8$ *cells/mL*. The improvement of droplet inkjet methods is achieved by draining excess water through a comb. In addition, a modified foam/lattice-based structure of the scaffold <1% *w/v* with a new support ribbon ensures cleaner and more precise biological object shaping. The updated RPS offers not only new hope for overcoming the shortage of organs for transplantation but also rejuvenation of the whole organism due to the forming of your own endocrine glands. It should be noted that albeit RPS is a project and has never used, it is a derivative of the time-tested methods and components of bioprinting. Potential of RPS for building multicellular tissue of high density and accuracy with a vascular system, with a width of 333 *mm* and a volume >1.7 *L* per hour at a layer thickness of 18 *μm*.

*Keywords:* 3D bioprinting, Bioadditive manufacturing, Tissue engineering, Biodegradable polymer, Roll Porous Scaffold

## 1. Introduction

Progress in 3D biofabrication, tissue engineering, and regenerative medicine holds great promise for anyone who wants to always be healthy, young, or rejuvenated.

Population aging and increased life expectancy have widened the gap between the shortage of tissue and organ transplants for transplantations "Karvinen et al. (2023)". The key to rejuvenation is not in nutrition, because if an old person and a child eat the same food, then the first one will continue to age, and the second one will grow. For this reason, it is logical to assume that hormones affect youth, and if their level is restored, then the whole body will look younger. The probability of rejection of bioprinted endocrine glands made from the man's DNA is minimal. These organs are much more complex than skin and cartilage and need vascularization to transport nutrients, oxygen, and waste "Leberfinger et al. (2019), Zhang et al. (2017)".

Achieving these goals with the help of modern bioprinters is difficult due to complex, heterogeneous biostructures with micro- and macrovascularization, innervation, differing in structural function, composition "Salg et al. (2022)" and mechanical properties.

Large arteries and their smaller branches (arterioles) have a layered wall structure, along which blood is transported to the capillary bed. Submillimeter sized capillaries consist of a single endothelial layer that provides permeability (gas exchange and nutrients). Macrovessels can be made-up in vitro, although with limited mechanical integrity "Freeman et al. (2019), Niklason et al. (2020)", while microvessels remain a challenge. Bioprinting of small capillaries is difficult since leading techniques allow the creation of vessels only >100 *μm* in diameter "Leberfinger et al. (2019)".

Appropriate mechanical properties and porosity are required to maintain the structure and growth of cells with a vasculature.

These specifications will depend on the rate and strength of the bioink crosslink, viscosity, and yield strength. Suitable plasticity of the bioink is necessary for printing, but at the same time, the shape must be maintained after printing to obtain sufficient dimensional integrity and mechanical strength.

DOI: 10.6977/IJoSI.202312_7(8).0004
V. Shulunov./Int. J. Systematic Innovation, 7(8),37-47(2023)

The RPS proposes to resolve listed difficulties fast and exactly at a low cost.

## 2. Methods and materials

### 2.1 Spiral coordinate system

Any 3D object can be transformed into a 2D stripe by the spiral coordinate system "Shulunov (2017a)" like a plane is transformed into a roll. This coordinate system defines a point's location in the volume with two and only one coordinate "Shulunov (2018)" instead of three in distinction from Cartesian one. The position of a voxel is determined by the length of the helix with tolerance depending on the constant h (the distance between successive turns). In RPS *h* is the height of the support ribbon, Fig. 1. Algorithms with their analysis "Shulunov (2017b), (2016a)" and software "Shulunov (2015), (2016b), (2016c), (2020)" for this coordinate conversion are described in detail in "Shulunov and Esheeva (2017c), (2017d)".

To make things clear Fig. 2 and Fig. 3 demonstrate the transformation of a tape filled with one and various components in order to form a multilayer tubular object from them in a wound roll.

Fig. 4 shows that schematic sequence of forming tubular branching object consists of different cell types.

### 2.2 Multicomponent support ribbon

One of the most important components of RPS technology consists of supporting fine sieve, porous, attachable, and auxiliary tapes (Fig. 5).

The basis of the supporting element is perforated 5 μm aluminum foil with holes of 7×7 $\mu m$ in size and a transparency of 49%.

The biodegradable polymer scaffold consists of combs 42×42×15 $\mu m$ in volume with an area of 37×37 $\mu m$ for placing 4 cells ∅10–15 $\mu m$ because of 5 $\mu m$ borders.

On the sides of the RPS ribbon are strips of incompressible material 18 $\mu m$ high to ensure a constant layer thickness.

A 3 $\mu m$ height attachable soluble tape with 49% transparency (7×7 $\mu m$ holes with 3 $\mu m$ selvedges) is used to stably delineate cell-filled helical layers.

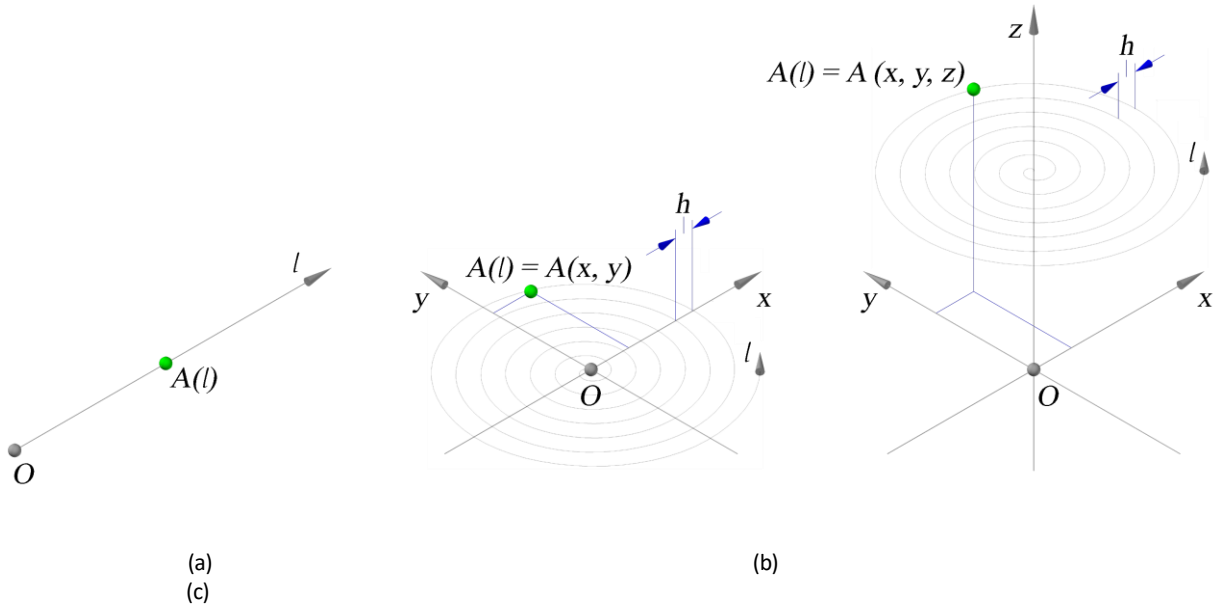


(a) (b) (c)

**Fig. 1.** Definition of "A" point's location in 1D (a), 2D (b) and 3D (c) spaces.

DOI: 10.6977/IJoSI.202312_7(8).0004
V. Shulunov./Int. J. Systematic Innovation, 7(8),37-47(2023)

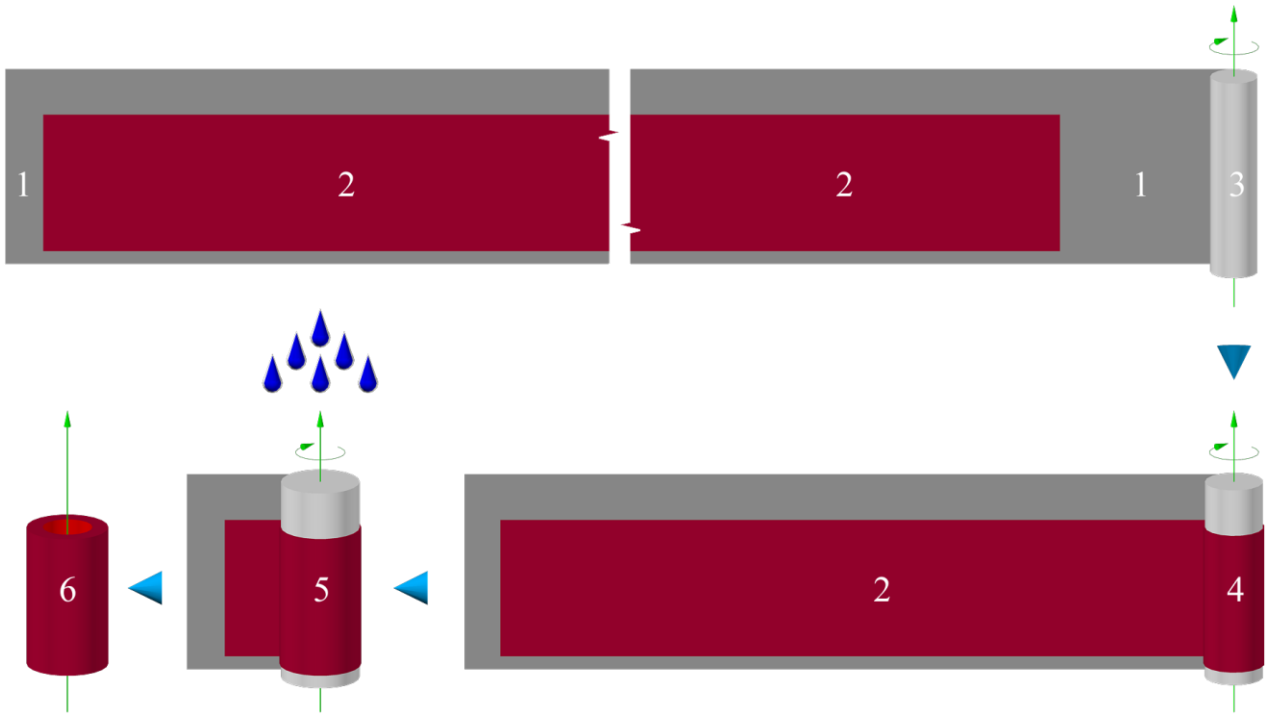


**Fig. 2.** Schematic sequence of transformation of a filled with cells water-soluble strip into a pipe object after its dissolution. (1) Empty scaffold ribbon, (2) Filled scaffold ribbon, (3) Roll forming object, (4) Tubular object inside the roll, (5) Almost formed object and support ribbon dissolving, (6) Object without scaffold.

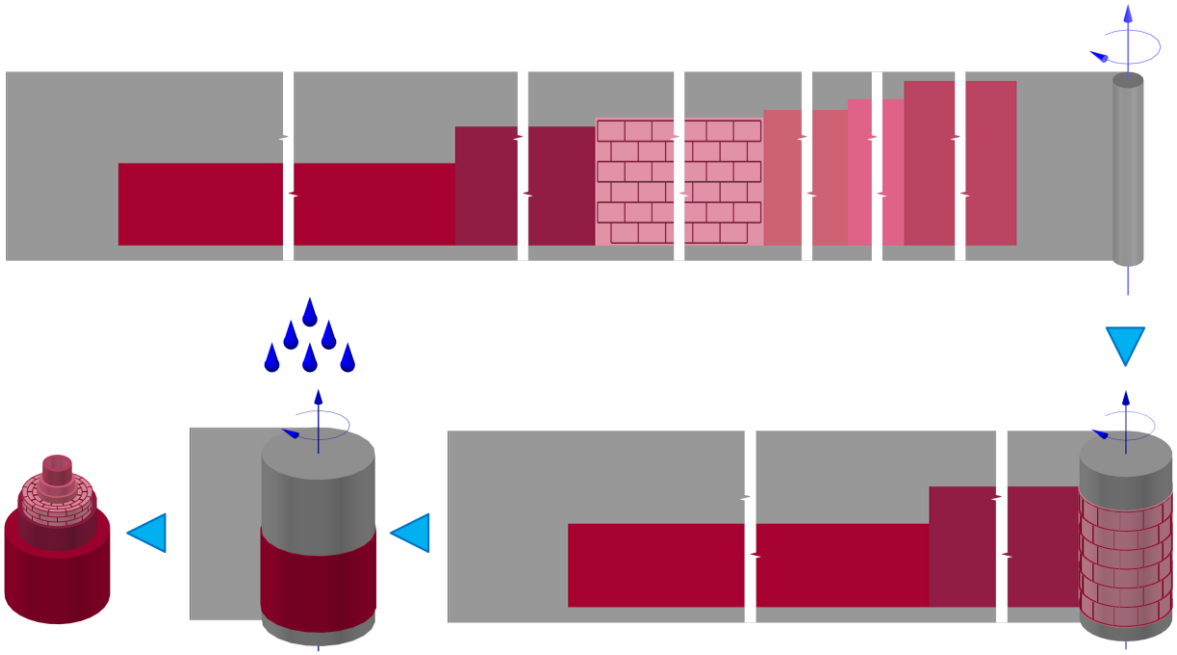

**Fig. 3.** Schematic sequence of formation of Tubular multilayer object of different cell types.

DOI: 10.6977/IJoSI.202312_7(8).0004
V. Shulunov./Int. J. Systematic Innovation, 7(8),37-47(2023)

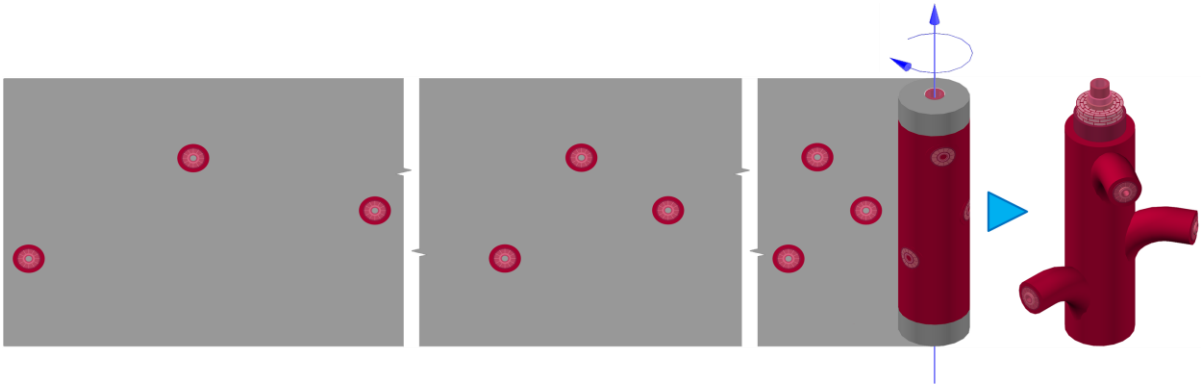

**Fig. 4.** Formation of a tubular branching object inside a roll.

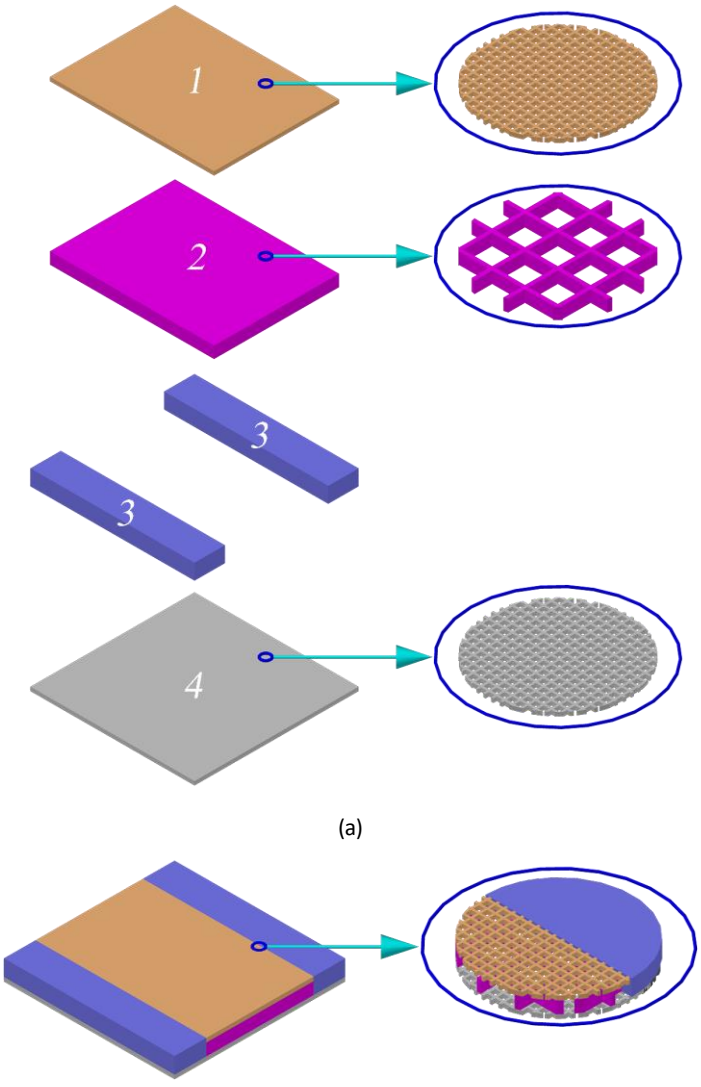


**Fig. 5.** Simplified scheme of RPS multilayer support ribbon. (a) Layers in order connection, (1) Attachable soluble tape (7×7 *μm* holes with 3 *μm* selvedges) for precise delineation of filled layers, (2) Biodegradable polymer scaffold for cells with combs 42×42×15 *μm*, (3) Incompressible material with a height of 18 *μm* for constant layer thickness, (4) 5 *μm* aluminum foil with holes of 7×7 *μm* (transparency of 49%) for drainage. (b) All layers together.

DOI: 10.6977/IJoSI.202312_7(8).0004
V. Shulunov./Int. J. Systematic Innovation, 7(8),37-47(2023)

### 2.3 Wide, high-speed inkjet printhead

The standard Kyocera Inkjet Printhead "KJ4B-1200" shoots 339 968 000 drops of 5 *pL* per second by 5 312 nozzles at 64 *kHz* on a width of 112.42 *mm* at a paper pulling speed of 80 *m/min* (~1.33 *m/s*) and a resolution of 1 200 *dpi* (21×21 $\mu m$ dot). Because each cell in the bioink is surrounded by a liquid volume of 1 000 *pL* (to guarantee fluidity) and ~200 drops are necessary to eject it out, by decreasing the speed of the tape to ~6.7 *mm/s* and removing excess water it is possible to reach cell quantity ~23 $(100/21)^2$, ~$23\times10^4$ and ~$1.13\times10^8$ on 100×100 $\mu m^2$, 1 $cm^2$ and in 1 $cm^3$ respectively for 20 $\mu m$ layers. Using a 3 $\mu m$ separation tape will lead to a layer thickness of 18 $\mu m$ and increase the cell density up to ~$1.26\times10^8$.

Therefore, the calculated performance for one usual serial piezo inkjet printhead is ~49 *mL/hour* (112.42×6.7×0.018×3 600).

The use of a line of 12 such heads makes it possible to form a biological object with a volume of ~0.58 *L* in an hour (cylinder ~112 *mm* high and ~81 *mm* in diameter).

Two parallel lines of these heads with an overlap of ~2.1 *mm* (100 nozzles) will provide a print width of ~223 *mm* and a throughput of ~1.15 *L/hour*.

### 2.4 ×100 increase of cell density in a porous matrix

The speed of inkjet Droplet Based Bioprinting (DBB) is higher than Extrusion Based Bioprinting (EBB) using pneumatic, piston, and screw driven printing, but the cell compactness is ~100 times lower. At first glance, DBB cannot outperform the cell concentration of EBB due to the bioink's high fluidity requirement. For sufficient fluidity without clogging the nozzles with bioinks, each cell ∅10–15 $\mu m$ (~0.5−1.8 *pL*) requires ~600–1 900 times larger volume of ambient liquid (Fig. 6).

However, computations show the chance of raising this feature of DBB by orders of magnitude when using RPS 3D bioprinter with a multicomponent ribbon. Fig. 7 depicts its simplified scheme.

To increase the density of conventional ink bioprinting by ~100 times and achieve a cell density of ~$1.26\times10^8$ cells per 1 *mL* for an 18 $\mu m$ layer, it is suggested to pass this flow through a fine sieve.

Separation of cells from the 1 000 *pL* flow occurs using a 37×37 $\mu m$ (1 369 $\mu m^2$) comb with 49% transparency surrounded by 5 $\mu m$ edging (the total square of the 7×7 $\mu m$ holes with 3 $\mu m$ borders will be ~671 $\mu m^2$). A drop with volume of ~5 *pL* (radius ~10.6 $\mu m$, cross-sectional ~353 $\mu m^2$) can easily pass through this area.

If a cell with a ∅10–15 $\mu m$ is pressed against the perforated bottom by the low pressure of the assisting fluid drainage system and a sequence of droplets, then on average it occupies ~123 $\mu m^2$ on the comb.

When 4 cells take ~491 $\mu m^2$ then ~878 $\mu m^2$ (1 369 - 491) will remain for the passage of excess water droplets through the perforated bottom of the comb with a total area of holes ~430 $\mu m^2$ (878×0.49).

### 2.5 Stabilization of the cells position in the roll of the bioprinted object

High fidelity of cell positioning, resolution, structure, and shape stability must be ensured during and after bioprinting within the required time for the cell culture period "Li et al. (2020), Kyle et al. (2017)".

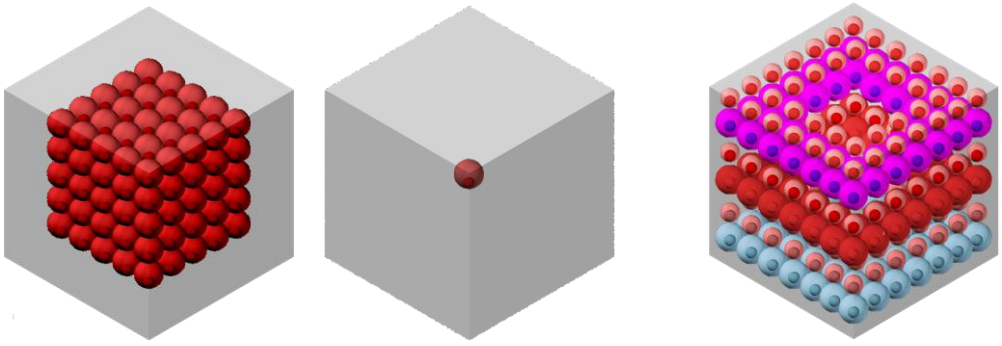


**Fig. 6.** Filling cells in a cube with a volume of 1 *nL*. (a) Adipose stem cells spheroid with minimum layer thickness of ~80 $\mu m$ "Zhang et al. (2015)", (b) Approximate cell density limit in bioink for 3D inkjet bioprinting, (c) Possibility of printing with cells

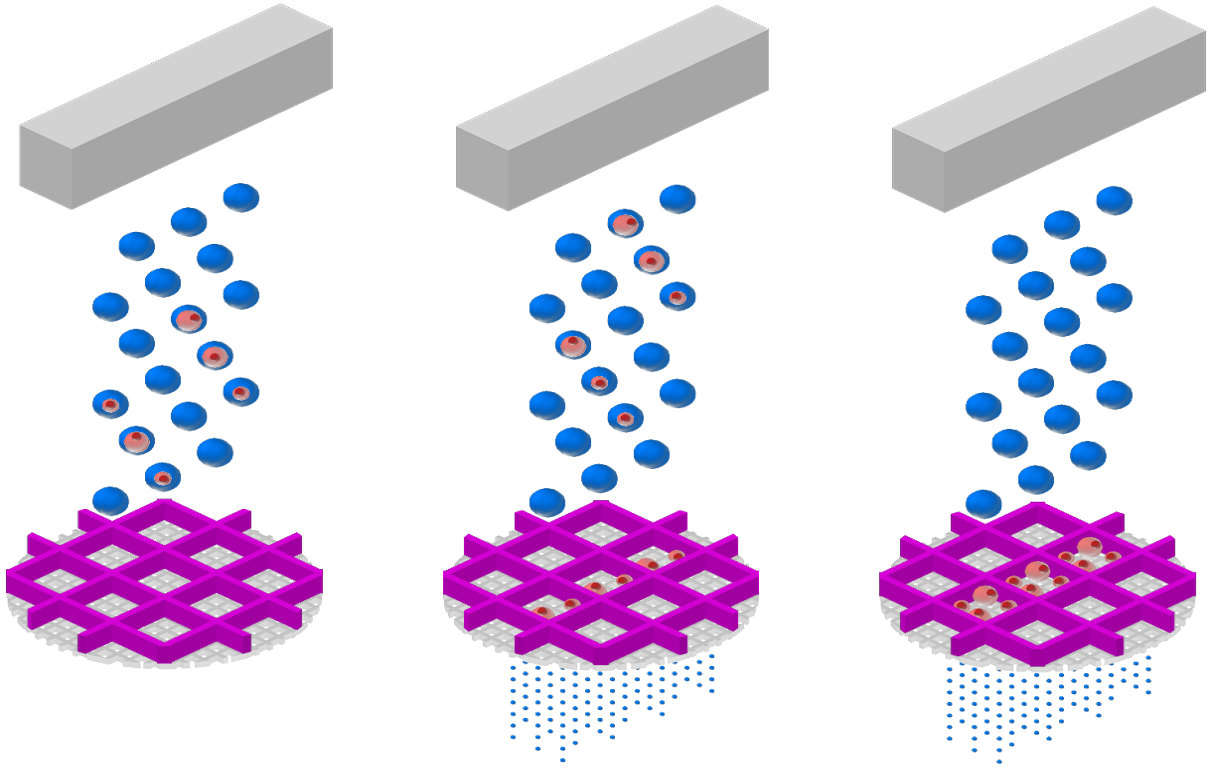


**Fig. 7.** Illustration of increasing the density of cell in the combs of the support ribbon by ~100 times up to ~$1.26\times10^8$ *cells/mL* using a fine sieve for DBB. (a) Combs before filling with cells. (b) Combs with partial filling and drainage. (c) Combs completely filled with cells during removal of excess water.

In RPS, a porous comb scaffold 15 $\mu m$ high and 5 $\mu m$ wide is used to limit cell displacement in the layer. Non-mixing of layers with each other is created by a supplementary porous soluble foam/lattice-based ribbon with a thickness of 3 $\mu m$ after placing the cells in the layer. The total admixture of the scaffold in the shaped biological object is <1%.

The ranges of distances between cells in 1 and neighboring layers are presented in Fig. 8. The distances between cells determine their interactions and tissue growth. For a pair of the smallest 10 $\mu m$ cells, the maximum distance is 8−17 $\mu m$, and for 15 $\mu m$ one 3−7 $\mu m$ in the adjacent layer and within its comb accordingly. The biggest 4 cells (∅7.5 $\mu m$) will occupy ~7 $pL$ of a 32 $pL$ (42×42×18 $\mu m$) comb voxel and there is enough space for them to swell and proliferate, after the bioink is placed into a porous scaffold, and allow therapeutics or waste products diffusion.

### 2.6 Basic RPS algorithm for 3D bioprinting

First, the tape is precisely rewound from roll (1) to roll (2) using rollers (3, 4) and a tension control system (5), Fig. 9. Then the drip filling system (6) fills it with various bioinks in accordance with the required tissue from a plurality of reservoirs installed above it. Excess ink water is removed by a drainage system (7) with a vacuum pumping system (13) into a tank (14). When the frame has been formed and filled with nutrient fluid from tank (12), it is covered with tape (9) separating the layers. The supporting foil is wound on a roll (10). The accuracy of the ribbon (reinforced and side-perforated like cinema film) winding is controlled by the frame's position and merging control

DOI: 10.6977/IJoSI.202312_7(8).0004
V. Shulunov./Int. J. Systematic Innovation, 7(8),37-47(2023)

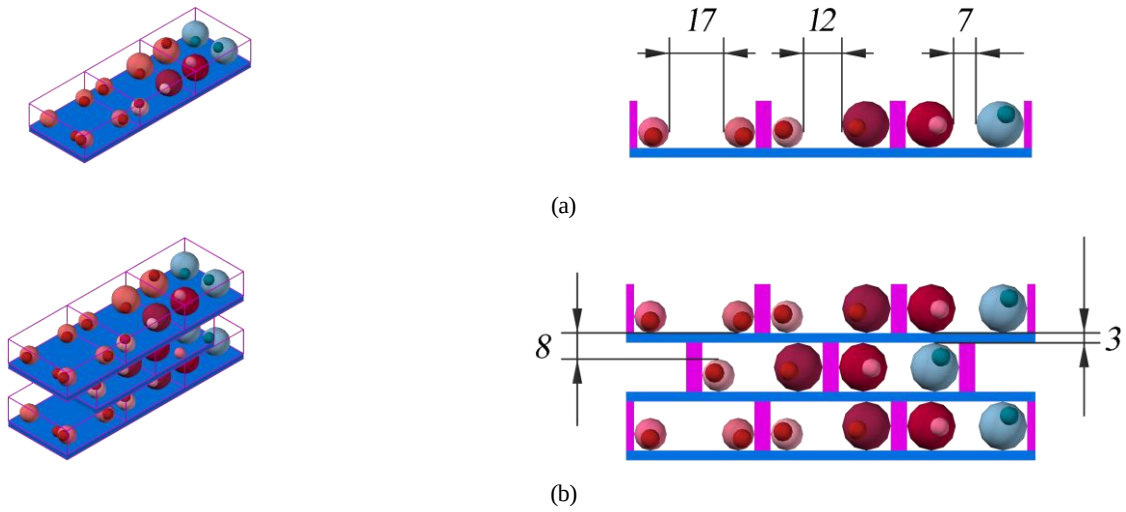


**Fig. 8.** Cells in a porous comb scaffold (isometric and side views), (a) the range of distance between cells 7−17 *μm* in 1 layer, (b) the range of distance between cells 3−8 *μm* in 3 layers.

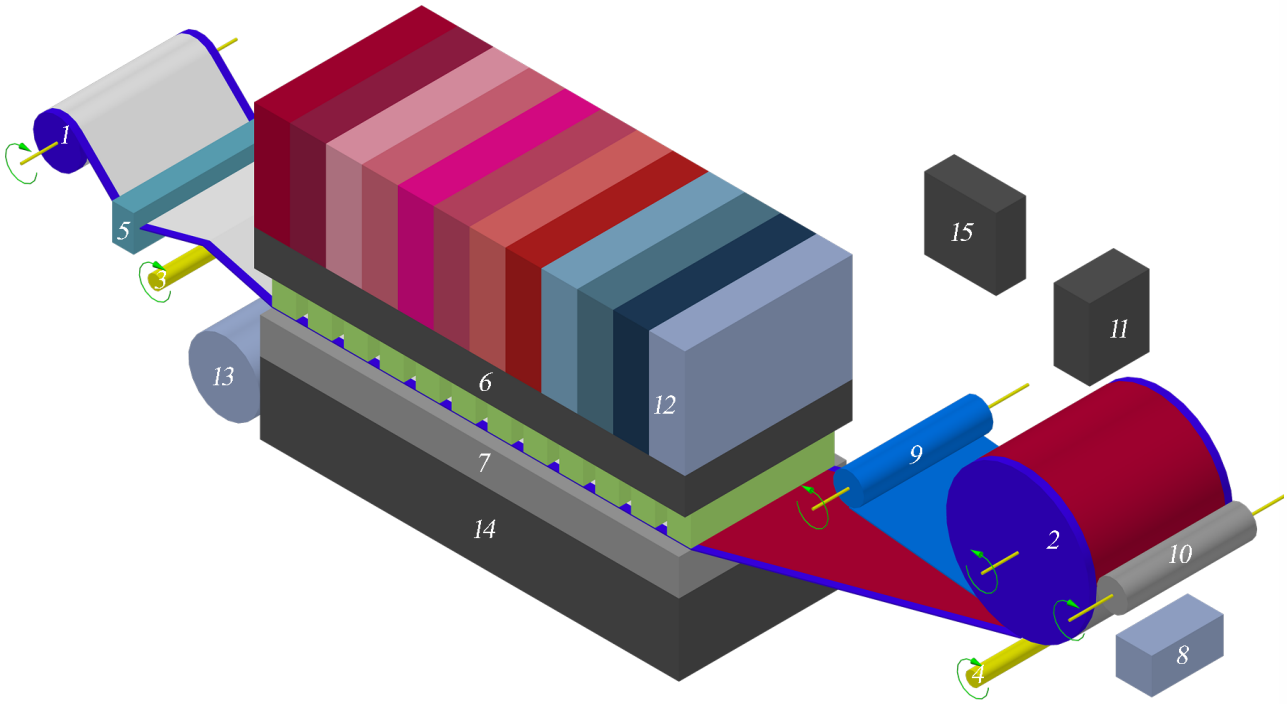


**Fig. 9.** Simplified general view of the enhanced RPS 3D bioprinter. (1) Scaffold roll, (2) Bio-object roll, (3) and (4) Extending rollers, (5) Supply roll unreeling tension control system, (6) Array with linear inkjet printheads with multiple reservoirs for each type of bioink, (7) Low pressure drainage system to remove auxiliary fluid, (8) Bio-object roll layer merging control system, (9) Attachable soluble tape for precise delineation of filled layers, (10) Aluminum foil with holes for drainage, (11) Frame position on the scaffold roll control system, (12) Nutrient fluid tank, (13) Vacuum pumping system, (14) Tank for excess water from bioink, (15) Component synchronization system.

systems (8) and (11). All these components are synchronized by system (15). Since the computed 3D CAD model of the bioprinting object is divided into frames, the position of all of them on the scaffold ribbon is known in advance by the length. The system verifies the actual and planned location for each frame. To correct possible distortion, the next one is shifted (by software) forward or backward according to the location of the marks, more details about "Frame position on the scaffold roll control system" are in the "Shulunov (2019)".

## 5. Results and discussion

Despite great advances in 3D bioprinting technologies for tissue engineering (without the lack of only planar cell-cell interactions), regenerative medicine, "organ on a chip" systems, and drug evaluation, there are still some challenges to be solved.

The currently dominant bioprinting methods compared in Table 1 do not allow solving a number of problems with exactly directed tissue mimic and providing transportation of nutrient and metabolic waste, blood supply and long-term survival of the cellular structure.

For example, it is difficult for EBB to print hollow tubes with an appreciable length-to-width ratio without using complex consumables in multiple printing processes.

EBB uses fugitive inks and endothelialization to print vascular networks. This sacrificial indirect bioprinting used to form hollow vessels consists of four steps: (1) solid sacrificial microfiber bioink is applied, (2) stromal cell-embedded hydrogel is applied to templated microfibers, (3) perfused channels are formed by selective fiber removal (e.g. temperature-induced phase transition, dissolution or mechanical extraction, etc.) under conditions suitable for the cells, and (4) functional vessels are built by seeding endothelial cells into the interior of the microchannels. This method is considered indirect bioprinting.

Alternatively, "Zhang et al. (2017), (2018)", channels are printed using direct bioprinting "Leberfinger et al. (2019)". These strategies for fabricating vascularization can be further divided into four groups "Salg et al. (2022)": 1) sacrificial bioprinting "Song (2018)", 2) sacrificial writing in functional tissue, SWIFT "Skylar-Scott et al. (2019)", 3) immersed bioprinting (reversible embedding of free-form suspended hydrogels, FRESH "Lee et al. (2019)") and 4) coaxial bioprinting "Gao et al. (2018)".

Innervation contributes to the development of tissues and organs, but also plays a central role as a tool for their functional control and modulation "Das et al. (2020)". Nerves provide the work of the auditory, skeletal or smooth muscles containing tissues (e.g. the stomach or bladder) "Das et al. (2020), Jammalamadaka and Tappa (2018)" and must have their own channels.

Complex three-dimensional organs require precise multicellular systems with vascular integration, which is currently not possible with traditional bioprinting methods.

The RPS has been designed to overcome all the problems mentioned above at a lower cost than the present dominant technologies.

The specifications of the new technology were developed or the simultaneous bioprinting multicellular tissue equipped with blood vessels with high exactness and density ~$1.26\times10^8$ *cell/mL* by matrix of fixed printheads for each type of cells (bioink of endothelial,

**Table 1.** Comparison of printing methods for bioprinting.

| **Bioprinting techniques** | **Extrusion** | **Laser** | **Inkjet** | **Enhanced RPS** |
|---|---|---|---|---|
| Cell diameter, $\mu m$ | 80–300 (cell spheroid) | 20–80 | 10–50 (1–100 *pL*) | |
| Resolution | Medium | High | | |
| Printing speed | Slow | Medium | Fast | |
| Cell density, *cells/mL* | ~$10^8$ | | <$5\times10^6$ | ~$1.26\times10^8$ |
| Cell viability, % | 97 | >97 | 85–98 | |
| Cost | Medium | High | Low | |

DOI: 10.6977/IJoSI.202312_7(8).0004
V. Shulunov./Int. J. Systematic Innovation, 7(8),37-47(2023)

**Table 2.** RPS 3D bioprinting based on inkjet technology.

| Title | Previous RPS | Enhanced RPS |
|---|---|---|
| Cell density, *cells/mL* | $<5\times10^6$ | $\sim1.26\times10^8$ |
| Layer thickness, *μm* | 20 | 18–20 |
| Print width, *mm* | 112–333 | |
| Performance, *L/hour* | >1.7 | |
| Print volume, *L* | ~5 | |
| | | |
| Transfer belt | Yes | No |
| Safety reeling protector | | |
| Transfer belt tension control system | | |
| Transfer belt refinement system | | |
| Low pressure drainage system to remove auxiliary fluid | No | Yes |
| Attachable soluble tape for precise delineation of filled layers | | |
| Aluminum foil with holes for drainage | | |
| Nutrient fluid tank | | |

smooth muscle, fibroblast, cartilage, collagen, osteoblasts, nerve and stem cells, etc.).

An array of three lines of 12×112.42 *mm* printheads with ~4.2 *mm* (2×100 nozzles) overlap will produce 333 *mm* wide bioobject with a performance of >1.7 *L/hour*.

At the same or better resolution than the previous version of bioprinting, enhanced RPS techniques have higher cell density and a simpler design (Table 2).

Form stability after printing is ensured by an easily dissolved porous ribbon scaffold (post-processing stabilization is not required) that withstands dynamic mechanical stress and promotes rapid vascularization with cell growth and proliferation.

Comb-shaped, side-reinforced tape, composed of soluble *nano*fibers and spongy biomaterials, creates a spatially mediated microenvironment and controlled intercellular distance with a high density of selected cells.

These scaffolds made of micron comb tape with 49% transparency ensure that droplets of cells do not move in their layer and do not mix with the neighboring one and do not flow out of the calculated places.

## 4. Conclusion

Enhanced RPS for the creation of biological objects is based on the use of linear matrices of multiple inkjet heads and a multicomponent support ribbon, which can be used to improve the biomodel of an organ tissue on a chip for testing new drugs on it.

A new RPS 3D bioprinter has been developed that outperforms dominant technologies. Its specifications are derived from commercially available inexpensive usual piezoelectric inkjet printer components suitable for bioinks as they do not heat cells. Expected properties for the manufacture of a biological object with a matrix of three lines of 12 printheads are: layer thickness of 18 *μm*, voxel comb resolution 42×42×18 *μm* for 4 cells with a size of ~10–15 *μm*, density of $\sim1.26\times10^8$ *cells/mL*, width 333 *mm* and throughput up to >1.7 *L/hour*.

The main workflow is simplified, requires fewer components, and improves purity of formed objects. The admixture of foam/lattice-based structure water soluble scaffold in the formed biological object is <1%.

The new technology proposes to create in vitro complicated organs like endocrine glands with precise multicellular systems equipped with vascular network

integration, which cannot be done by traditional leading bioprinting technologies.

The paper shows ways to overcome the main technological barriers of 3D bioprinting for organs and significantly accelerate the bioproduction of large complicated multilevel cellular structures, tissue engineering, organ patch, or organ transplants for transplantations, regenerative and rejuvenation medicine in the near future.

**Disclosure statement**

No potential conflict of interest was reported by the authors.

## References

Das, S., Gordi´ an-V´elez, W.J., Ledebur, H.C., Mourkioti, F., Rompolas, P., Chen, H.I., Serruya, M.D., & Cullen, D.K. (2020). Innervation: the missing link for biofabricated tissues and organs, NPJ Regen. Med. 5 (1) 11. doi.org/10.1080/17452759.2017.132513

Freeman, S., Ramos, R., Chando, P.A., Zhou, L., Reeser, K., Jin, S., Soman, & P., Ye, K. (2019). A bioink blend for rotary 3D bioprinting tissue engineered small-diameter vascular constructs, Acta Biomater. 95, 152–164.

Jammalamadaka, U., Tappa, K. (2018). Recent advances in biomaterials for 3D printing and tissue engineering, J. Funct. Biomater. 9 (1) 22.

Karvinen, J., Kellomäki, M. (2023) Design aspects and characterization of hydrogel-based bioinks for extrusion-based bioprinting, Bioprinting, Volume 32, e00274, ISSN 2405-8866, https://doi.org/10.1016/j.bprint.2023.e00274.

Kyle, S., Jessop, Z.M., Al-Sabah, A., & Whitaker I.S. (2017). 'printability' of candidate biomaterials for extrusion based 3D printing: state-of-the-art, Adv. Healthc. Mater. 6 (16), 1700264.

Leberfinger, A.N., Dinda, S., Wu Y., Koduru, S.V., Ozbolat V., Ravnic D.J., & Ozbolat I. T. (2019). Bioprinting functional tissues, Acta Biomater. 95, 32–49.

Li, J., Wu, C., Chu, P.K., & Gelinsky, M. (2020). 3D printing of hydrogels: rational design strategies and emerging biomedical applications, Mater. Sci. Eng. R Rep. 140, 100543.

Niklason, L.E., Lawson, J.H. (2020). Bioengineered human blood vessels, Science 370 (6513), eaaw8682.

Salg, G.A., Blaeser, A., Gerhardus, J.S., Hackert, T., & Kenngott, H.G. (2022). Vascularization in bioartificial parenchymal tissue: bioink and bioprinting strategies, Int. J. Mol. Sci. 23 (15) 8589.

Shulunov, V.R. (2015). The program spiral converting parallel similar objects into a linear sequence [Programma spiral'nogo preobrazovaniya parallel'no podobnykh ob'ektov v linejnuyu posledovatel'nost']. Certificate of state registration of computer programs No. 2016613199(RU), 21 Dec 2015. (in Russian). doi: 10.13140/RG.2.2.17982.05446

Shulunov, V.R. (2016a). Algorithm for converting 3D objects into rolls using spiral coordinate system, Virtual and Physical Prototyping. 11 (2) 91–97. https://doi.org/10.1080/17452759.2016.1175360.

Shulunov, V.R. (2016b). Linear Spiral Convertor for 3D Objects into a Ribbon [Linejno Spiral'nj Convertor slojov3D ob'ektov v lentu]. Certificate of State Registration of Computer Programs No. 2017614132(RU), 07 Dec 2016. (in Russian). doi: 10.13140/RG.2.2.29313.25443/1

Shulunov, V.R. (2016c). The Program Spiral Converting Solids of Revolution into a linear Sequence [Programma Spiral'nogo Preobrazovaniya Tel vraschenia v linejnuyu Posledovatel'nost']. Certificate of State Registration of Computer Programs No. 2017614186(RU), 26 Oct 2016. (in Russian). doi: 10.13140/RG.2.2.15570.35523/1

Shulunov, V.R. (2017a). Transformation of 3D object into flat ribbon for RPS additive manufacturing technology. Rapid Prototyping Journal, Vol. 23 No. 2, pp. 273-279. doi: 10.1108/RPJ-11-2015-0164.

Shulunov, V.R. (2017b). Comparison of algorithms for converting 3D objects into rolls, using a spiral coordinate system, Virtual and Physical Prototyping. 12 (3) 249–260. https://doi.org/10.1080/17452759.2017.1325132.

Shulunov, V.R., Esheeva, I.R. (2017c). Accelerated algorithm for solids of revolution converting into ribbon by spiral coordinate system, International Journal of Intelligent Engineering and Systems. Vol. 10 (3) 117–125. doi: 10.22266/ijies2017.0630.13

Shulunov, V.R., Esheeva, I.R. (2017d). A linear algorithm for conformal 3D-to-flatness coordinates conversion, Virtual and Physical Prototyping. 12 (1) 85–94. https://doi.org/10.1080/17452759.2016.1276820.

Shulunov, V.R. (2018). Advanced Roll Powder Sintering additive manufacturing technology, Int. J. Interact. Des. Manuf. https://doi.org/10.1007/s12008-018-0475-7.

Shulunov, V.R. (2019). A novel Roll Porous Scaffold 3D bioprinting technology, Bioprinting, Volume 13, e00042, https://doi.org/10.1016/j.bprint.2019.e00042.

Shulunov, V.R. (2020). Parallel slicer of STL files for Roll Powder Sintering additive technology [Parallel'nyy slayser STL faylov dlya Roll Powder Sintering additivnoy tekhnologii]. Certificate of State Registration of Computer Programs No. 2020618781 (RU), 15 May 2020. (in Russian). doi: 10.13140/RG.2.2.22176.35848

Zhang, Y.S., Yue, K., Aleman, J., Mollazadeh-Moghaddam, K., Bakht, S.M., Yang, J., Jia, W., Dell'Erba, V., Assawes, P., Shin, & S.R., et al. (2017). 3D bioprinting for tissue and organ fabrication, Ann. Biomed. Eng. 45 (1) 148–163.

Zhang, K., Yan, S., Li, G., Cui, L. & Yin, J. (2015). In-situ birth of MSCs multicellular spheroids in poly (L-glutamic acid)/chitosan scaffold for hyaline-like cartilage regeneration. Biomaterials 71, 24–34 doi: 10.1016/j.biomaterials.2015.08.037

## AUTHOR BIOGRAPHIES

**Vyacheslav R. Shulunov** is a researcher at the Institute of Physical Materials Science of the Siberian Branch of the Russian Academy of Science, Ulan-Ude, Russia since 1997. In 1992 he entered the Buryat Branch of the Novosibirsk State University. In 1997 graduated from the Buryat State University, Ulan-Ude Russia. Vyacheslav Shulunov received his Ph.D. degree in Thermal Physics and Theoretical Heat Engineering in 2002 from the East Siberia State University of Technology and Management. The author of 3 patents of the Russian Federation, 5 certificates of state registration of the program and databases, 11 Web of Science and Scopus publications. Scopus *h*-index: 5 with 1 co-author in 2 publications. https://www.scopus.com/authid/detail.uri?authorId=56536940900. ORCID 0000-0002-0114-7739. He is currently a resident of the Skolkovo innovation center. CEO A1 LLC.